Durham University

Durham Research Online

Deposited in DRO:

26 September 2012

Version of attached file:

Published Version

Peer-review status of attached file:

Peer-reviewed

Citation for published item:

Al-Attar, H.A. and Monkman, A.P. (2011) 'Solution processed multilayer polymer light-emitting diodes based on different molecular weight host.', Journal of applied physics., 109 (7). 074516.

Further information on publisher's website:

http://dx.doi.org/10.1063/1.3569831

Publisher's copyright statement:

© 2011 American Institute of Physics. This article may be downloaded for personal use only. Any other use requires prior permission of the author and the American Institute of Physics. The following article appeared in Al-Attar, H.A. and Monkman, A.P. (2011) 'Solution processed multilayer polymer light-emitting diodes based on different molecular weight host.', Journal of applied physics., 109 (7). 074516 and may be found at http://dx.doi.org/10.1063/1.3569831

Use policy

The full-text may be used and/or reproduced, and given to third parties in any format or medium, without prior permission or charge, for personal research or study, educational, or not-for-profit purposes provided that:

- a full bibliographic reference is made to the original source
- a link is made to the metadata record in DRO
- the full-text is not changed in any way

The full-text must not be sold in any format or medium without the formal permission of the copyright holders.

Please consult the full DRO policy for further details.

Durham University Library, Stockton Road, Durham DH1 3LY, United Kingdom
Tel : +44 (0)191 334 3042 | Fax : +44 (0)191 334 2971
https://dro.dur.ac.uk

Solution processed multilayer polymer light-emitting diodes based on different molecular weight host

Hameed A. Al-Attar and Andrew P. Monkman

Citation: J. Appl. Phys. **109**, 074516 (2011); doi: 10.1063/1.3569831
View online: http://dx.doi.org/10.1063/1.3569831
View Table of Contents: http://jap.aip.org/resource/1/JAPIAU/v109/i7
Published by the American Institute of Physics.

Related Articles

White top-emitting organic light-emitting diodes employing tandem structure
APL: Org. Electron. Photonics 5, 216 (2012)

White top-emitting organic light-emitting diodes employing tandem structure
Appl. Phys. Lett. 101, 133302 (2012)

GaN-based light emitting diodes with micro- and nano-patterned structures by femtosecond laser nonlinear decomposition
Appl. Phys. Lett. 101, 131103 (2012)

Quantum-confined stark effect in localized luminescent centers within InGaN/GaN quantum-well based light emitting diodes
Appl. Phys. Lett. 101, 121919 (2012)

Performance and polarization effects in (112) long wavelength light emitting diodes grown on stress relaxed InGaN buffer layers
Appl. Phys. Lett. 101, 121106 (2012)

Additional information on J. Appl. Phys.

Journal Homepage: http://jap.aip.org/
Journal Information: http://jap.aip.org/about/about_the_journal
Top downloads: http://jap.aip.org/features/most_downloaded
Information for Authors: http://jap.aip.org/authors

ADVERTISEMENT

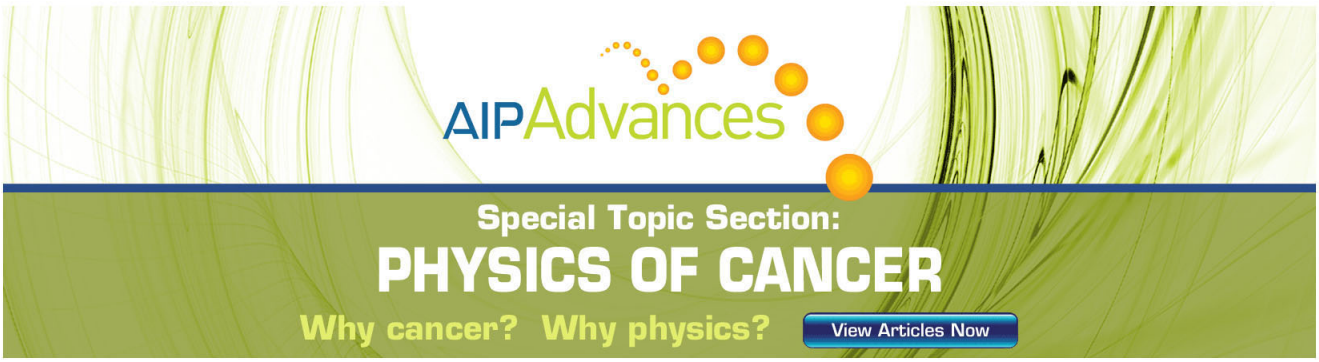

Downloaded 26 Sep 2012 to 129.234.252.67. Redistribution subject to AIP license or copyright; see http://jap.aip.org/about/rights_and_permissions

Solution processed multilayer polymer light-emitting diodes based on different molecular weight host

Hameed A. Al-Attar[a] and Andrew P. Monkman
Organic Electroactive Materials Research Group, Department of Physic, University of Durham, South Road, Durham DH1 3LE, United Kingdom

(Received 15 November 2010; accepted 29 January 2011; published online 12 April 2011; publisher error corrected 14 April 2011)

Solution processed multilayer polymer light-emitting diodes (PLEDs) based on different molecular weight host have been investigated. A PLED based on high molecular weight poly (vinyl carbazole) PVKH and low molecular weight poly (vinyl carbazole) PVKL, doped with iridium, tris (2-phenylpyidine) $Ir(ppy)_3$ as a host-guest emitting layer (EML), shows a dramatic increase in device efficiency. When the PVKH was used as a hole transport electron blocking layer (HT-EBL), effective electron blocking was achieved, which leads to an increase exciton population in the phosphorescent zone. The use of low molecular weight PVKL as a host material in the top layer prevents barrier formation for hole transport from the poly(3,4-ethylenedioxy-thiophene) (PEDOT)–EBL to the EML. External quantum efficiency of 11%, current efficiencies of 38 cd/A, power efficiency of 13 lm/W and brightness of 7000 cd/m^2, were obtained. The effect of the PVKH layer on the electrical and optical device characteristics was investigated. Simulation of the optical outcoupling using SETFOS 3.1 software is in agreed with the observed results and allowed us to predict the emissive dipole location and distribution in the EML layer. The effect of the PVKH on the exciton quenching by the electrodes was also investigated using time resolved fluorescence photon counting, which indicates weak exciton quenching by the PEDOT layer and the device enhancement predominantly achieved by exciton confinement in the emissive layer. © *2011 American Institute of Physics*. [doi:10.1063/1.3569831]

I. INTRODUCTION

Large area and high efficiency polymer light-emitting diodes (PLEDs) and solar cells (SCs) have attracted great interest due to potential low cost solution processability by classical printing methods. The most common polymer device structure is a single layer active material that is most probably a copolymer or a blend to achieve the desire emission wavelength and to balance the injected charge carriers. However, different electron and hole mobility, nonideal electron and hole injection, quenching by electrodes,[1] and confinement in the active region[2] make single layer PLEDs low efficiency and short lifespan devices for many applications. One answer to these problems can be to make multilayer devices by thermal evaporation of low molecular organic materials or by an evaporating electron transport layer on the top of the spin-coated polymer active layer. Multilayer Organic Light Emitting Diodes (OLEDs) are more efficient than single layer types because one can engineer the outer layers next to the electrodes to enhance hole and electron injection; this reduces the turn-on voltage in case of OLED or facilitate carrier collections in case of organic solar cells. Furthermore, these layers may also act to block the counter charge carrier confining electron-hole pairs in the active region and increasing the probability of generating emissive excitons that are essential for high quantum efficiency OLEDs. In an effort to emulate this, multilayer solution processable PLEDs have been suggested by many based on water-alcohol-soluble polymers salts[3–5] or inorganic ionic materials.[6] Other methods like thermally or UV cross-linked hole transporting layer,[7–9] insoluble interlayer of various conjugated polymers forms upon annealing,[2,10] and intermediate liquid buffer layer[11] have also been used to spin-coat multilayer devices. High molecular weight PVK has also been used as a hole transport layer in a blue emitting polymeric light emitting devices, where blue emissive layer spin on the top of it.[12] Interfacial PVK layers have also been shown to affect the β-Phase of poly(9,9-dioctylfluorene) due to morphology changes in the interface.[13]

In this paper, we present a simple and efficient solution processed multilayer structure polymer light emitting diode by incorporating different molecular weight polymers. We demonstrate that the solubility as a function of the polymer molecular weight can be used to spin-coat multilayer PLED devices. As an example, we have fabricated PLEDs based on high molecular weight poly (vinyl carbazole) PVKH as a hole transport/electron blocking layer and low molecular weight poly (vinyl carbazole) PVKL, doped with $Ir(ppy)_3$ as a host-guest emitting layer. The effect of the PVKH on the optical and device efficiency has been investigated. Although the device fabricated had excellent characteristics, these PLEDs are intended as a proof of concept, therefore only a comparison method was considered here; a complete optimization for performance (dopant concentration, injection process, etc.) has not been made at this stage.

II. MATERIALS AND METHODS

It is well known that PVK is a good hole transport polymer. In addition, PVK has also been used extensively as a

[a]Author to whom correspondence should be addressed. Electronic mail: h.a.al-attar@durham.ac.uk.

 © 2011 American Institute of Physics

Downloaded 26 Sep 2012 to 129.234.252.67. Redistribution subject to AIP license or copyright; see http://jap.aip.org/about/rights_and_permissions

host material for a number of phosphorescent dopants due to its high triplet energy level 2.6-2.7 eV.[14] PVK of various molecular weights was obtained from Sigma-Aldrich{Possible Ad} and used without further purification.

All devices were fabricated on indium tin oxide (ITO)-coated glass substrates of thickness 125 nm and possessing a sheet resistance of 16 Ω/□. Poly(3,4-ethylenedioxy-thiophene) in poly(styrenesulfonic acid) (PEDOT:PSS), obtained commercially from Bayer A.G. Germany, was spin coated at 1500-2500 rpm for 60 s to produce a ~40-70 nm thick hole-injection layer (HIL). These HIL-coated substrates were then annealed at 200 °C for 3 min on a hot plate to remove any residual water. A chlorobenzene solution of various concentrations (mg/ml) of a high molecular weight poly (vinyl carbazole) PVKH (Mw = 1100000) (Sigma-Aldrich) was spin-coated at 2500 rpm to give 12–52 nm as a hole transport/electron blocking layer. This second layer was annealed at 120 °C for 10 min to remove the solvent and left to cool down to room temperature. A toluene solution of low molecular weight of PVKL (Mw = 43000-90000) (Sigma-Aldrich) and 40% w/w of an electron transport material, 2-(4-biphenylyl)-5-(4-tetrbutyl-phenyl)-1, 3, 4-oxadiazole (PBD), doped with 8% w/w of the iridium, tris (2-phenylpyidine) $Ir(ppy)_3$ was prepared. The solution was filtered with 0.45 μm pore filter and spin-coated at 2500 rpm on the top of the PVKH and baked for 10 min at 120 °C; this acts as a light-emitting layer (EML). Each sample had a shadow mask applied to produce four identical devices of area 4×5 mm; the samples were then introduced into a nitrogen glovebox, where 4 nm barium cathodes were evaporated onto the device at a rate of ~1 Å/s under vacuum at a pressure of ca. 1×10^{-6} mm Hg. This was followed by the deposition of a 100 nm capping layer of aluminum under the same evaporation conditions. For unipolar (hole only) devices, 60 nm gold layer was evaporated instead of the Ba/Al cathode. All samples are encapsulated inside the glovebox using DELO UV cured epoxy (Katiobond) and capped with 1.5×1.5 microscope glass then exposed to UV light for 3 min. Similar procedures were used to fabricate single layer PVKH (chlorobenzene) or PVKL (toluene) and double layers PVKH (chlorobenzene)/PVKL (toluene) on $SiSiO_2$ substrates for film thickness and optical constant measurement using a J. A. Woollam Ellipsometer.

The effect of EML emission quenching by various interfaces was investigated using an analogus emission polymer, poly(spiribifluorene) (PSBF). PSBF was dissolved in toluene and used as an EML layer, which can be spin-coated on the PVKH layer. A set of different multilayer configurations were prepared on glass or glass/ITO substrates as indicated in Table II.

Current-voltage (*I-V*) characteristics and the emission intensities were measured in a calibrated integrating sphere with data acquisition controlled using a home-written NI LabView program that controlled Agilent Technologies{Possible Ad} 6632B power supply. The electroluminescence (EL) spectra were measured using an Ocean Optics{Possible Ad} USB 4000 CCD spectrometer supplied with 400 μm UV/Vis fiber optic.

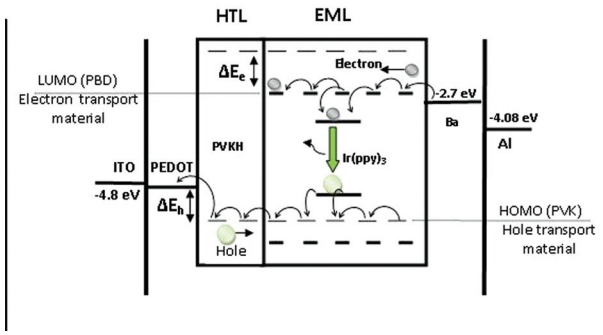

Scheme 1. (Color online) The device architecture and the schematic energy level diagrams for materials used in the device.

Fluorescence emission quenching was measured using time resolved fluorescence photon counting. The excitation wavelength at 372 nm was generated from the second harmonic frequency of Ti-sapphire laser operating at 76 MHz.

III. RESULTS AND DISCUSSION

A. Device structure and energy level diagram

The device architecture and the schematic energy level diagrams for materials used in the device are shown in Scheme 1. The well defined multilayer structure was confirmed using ellipsometry; the total multilayer film thickness was found to be equal to (± 3 nm) that of the sum of the two individual film thicknesses. This indicates that the second layer does not dissolve the first layer to any great extent. The insolubility of the high molecular weight PVK (PVKH) film in toluene was measured using ellipsometry, which showed that a 110 nm annealed film of the high molecular weight PVKH immersed in toluene for 1 min reduced by 5 nm only, and no delaminating was found. The PVKH layer thickness reduction was <2 nm when the second layer was spin-coated from the toluene solution. Therefore a precise time control of the following EML is necessary for obtaining perfectly isolated layers with repeatable results. Further confirmation of bilayer formation was proved from device characterization, which is discussed in the following text.

B. Device emission characteristics

In a single EML layer device, consisting of PVK and PBD only, the injected electrons from the cathode are mainly captured and transported by the PBD because the LUMO level of the PBD at −2.4 eV is the closest to the Ba work function at −2.7 eV and also because PBD is an efficient electron transport material.[15] At the anode side, the nearest HOMO energy level to the PEDOT:PSS at −5.2 eV is the HOMO level of the PVK at −5.8 eV. Our EL emission measurements (Fig. S1)[16] of these devices show the emission peak centered at 430 nm (2.88 eV), which is an exciplex emission that forms between electrons at the LUMO level of the PBD with holes at the HOMO level of the PVK and not at 400 nm that characterize the emission of the excimer formed between the LUMO-HOMO levels of the PVK

Downloaded 26 Sep 2012 to 129.234.252.67. Redistribution subject to AIP license or copyright; see http://jap.aip.org/about/rights_and_permissions

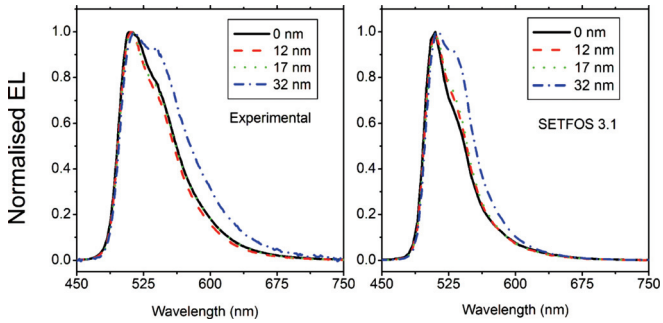

FIG. 1. (Color online) Normalized EL spectra for multilayer devices at variable HTL (PVKH) layer thickness (0, 12, 17.4, and 33 nm) with a fixed EML thickness of 50 ± 3 nm. (b) EL spectra profile obtained by simulation using SETFOS 3.1. Device structure is: G/ITO/PEDOT: PSS/PVKH(x nm)/PVKL:PBD:Ir(ppy)$_3$ (50 ± 3 nm)/Ba/Al.

molecular units.[17,18] By doping this system with Ir complex, that is, Ir(ppy)$_3$, electrons from PBD are strongly trapped at the LUMO (triplet spin multiplicity) of the Ir(ppy)$_3$, (−2.8 eV); similarly holes at PVK are trapped at the HOMO level of the Ir(ppy)$_3$ (−5.22 eV), generating phosphorescent excitons, and only EL emission from Ir(ppy)$_3$ centered at 512 nm (2.42 eV) was observed with no emission from the PVK excimer at 400 nm or from the exciplex at 430 observed even at low (<1%) Ir(ppy)$_3$ concentration.

Introducing a PVKH layer does not alter the EL spectra emission peak; this indicates no exciplex or electroplex emission generated at the interface between PVKH and PVKL, but it may alter the EL emission profile due to microcavity effects. The EL emission of the devices with various PVKH layer thicknesses (x), in the device architecture; glass/ITO/PEDOT:PSS/PVKH (x nm)/PVKL:PBD (40%): Ir(ppy)$_3$ (8%) (50 ± 3 nm)/Ba (4 nm)/Al (100 nm) is shown in Fig. 1(a). A thicker PVKH layer shows a broadening of the EL spectra on the red side of the emission band. Such observations are attributed to the interference effects due to the changes in the optical path length where the change in EL spectrum is measured at normal to the surface.[19,20] Broadening of the PL spectra on the red side of the emission band was also observed when the device was optically excited; this confirms the cavity interference effect. Optical simulation using SETFOS 3.1 software[21] can qualitatively describe the effect of PVKH on EL spectra emission and also can predict the radiating dipole density location and distribution. Figure 1(b) shows the corresponding simulated data to the experimental EL spectra of Fig. 1(a). The redshift in the simulated emission spectra is observed in a very similar manner to that obtained from the experimental measurement. However, the simulation fails to fit the long wavelength side of the EL spectra, and this is in part due to excimer emission contribution from Ir(ppy)$_3$ at 8% w/w concentration,[22] which is not included in the optical simulation. Fit of the dipole distribution to the experimental spectra indicates that the dipole location and distribution should be close to the interface between the PVKL/PVKH (Fig. S2)[16] to obtain the simulation spectral of Fig. 1(b). The simulation also shows that the maximum luminous efficacy of radiation occurs for PVKH thickness between 25 and 30 nm (Fig. S3).[16]

EL broadening in the red side of the spectra was also observed when the dopant concentration was increased;[23] this indicates that the dopant concentration may also change the emissive zone due to charge trapping in the dopants.[24,25] However, a full knowledge of exciton distribution inside the EML layer required a full electronic-to-optical coupling simulation.

C. Electrical characteristics and device performance

The effect of the PVKH layer on the electrical characteristics of the organic light emitting device based on molecularly doped polymers requires knowledge of the mechanisms by which charge carriers are generated, trapped, transported, and combined in the EML blended layer. The electrical characteristics of the devices with different PVKH thicknesses are shown in Fig. 2; here the current-voltage (I-V) and inset current-field (I-F) characteristics for device condition are (a) fixed EML thickness (50 ± 3 nm) and variable PVKH thickness (0, 12, 17.4, 33 nm) and (b) fixed PVKH (20 ± 2 nm) and variable EML thickness (27, 38.5, 51 nm). As the PVKH thickness increases [Fig. 2(a)], the device current decreases, but the associated external quantum efficiency (EQE %) and current efficiency (cd/A) increases (Fig. 3). This characteristic indicates that the probability of generating exciton is increased. The lower dark current density measured at thicker PVKH devices indicates an increase in the trapping probability at the complex sites yielding more efficient exciton generation. The electron mobility of the emissive layer [PVKL:PBD:Ir(ppy)$_3$] is dominated by the PBD (2×10^{-5} cm^2/Vs)[20] and is higher than the hole mobility of the PVKH (the measured PVK hole mobility range from 4.8×10^{-9} to

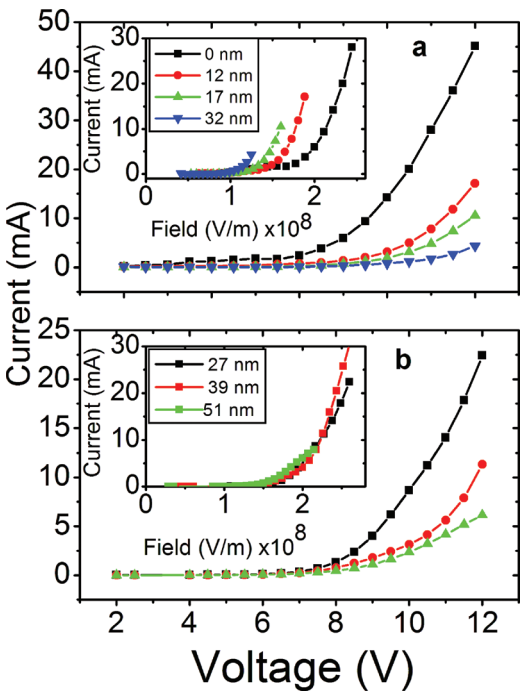

FIG. 2. (Color online) Current-voltage (I-V) and current-field (I-F) characteristics for (a) fixed EML thickness (50 ± 3 nm) with variable PVKH thickness (0, 12, 17, 32 nm) and (b) fixed PVKH (20 nm) with variable EML thickness (27, 39, 51 nm). Thicker layer thickness shows lower current.

Downloaded 26 Sep 2012 to 129.234.252.67. Redistribution subject to AIP license or copyright; see http://jap.aip.org/about/rights_and_permissions

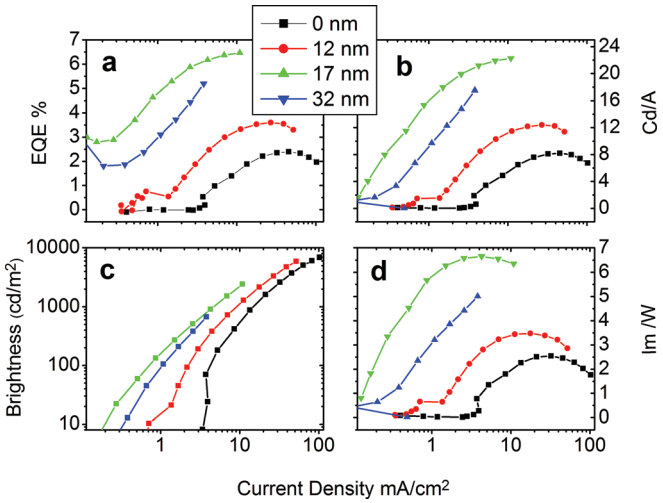

FIG. 3. (Color online) (a) External quantum efficiency, (b) device current efficiency (cd/A), (c) brightness (cd/m^2), and (d) luminous efficacy of a source (lm/W) as a function of current density (mA/cm^2) of the solution processed multilayer device structure shown in Scheme 1 for different PVKH thickness (0, 12, 17, and 32 nm).

10^{-6} cm^2/Vs, depending on the electric field strength).[26] Furthermore, with the 40% w/w concentration of the PBD, a percolation network can form channels for the electron transport efficiently to the PVKH interface, which reduces the probability of electron trapping. Because both HT/EBL and EML are made from PVK, this structure benefits from the smooth hole transport across the device layers without hindrance. On the other hand, the electron's transport by the PBD and Ir complex is blocked by the PVKH layer because a potential barrier of 0.4-0.6 eV has to be overcome by the electron located in the PBD LUMO level to reach the LUMO level of the PVKH at −2.2 eV. These mechanisms are illustrated in Scheme 1. Therefore electrons are expected to accumulate at the interface between the PVKH and PVKL:PBD:Ir(ppy)$_3$, giving rise to more efficient exciton generation, and a significant enhancement in the device performance can be obtained. This explanation is supported by the simulation of the EL emission spectra (Fig. 1) which indicates that the experimental EL emission profile is only observed in the case of the emissive dipole location at the interface between the PVKH/PVKL. The PVKH layer also keeps the emissive zone confined in the EML layer away from the electrodes, preventing quenching by the PEDOT.[27] With increasing PVKH thickness, the electrons accumulate more in the emissive region, generating a high local field across the PVKH layer leading to device breakdown. The breakdown voltage depends critically on the PVKH layer thickness, limiting device thickness to <32 nm. As the PVKH layer thickness increases, the resistance to hole transport increases too (PVK hole resistivity is around 10^9 Ω cm[26]); the electron population therefore outnumbers that of holes, and the device efficiency tends to decline. Plotting the current as a function of the field strength, Fig. 2(a) inset, we find that the device operating field is lower in the case of the bilayer devices and decreases as the PVKH thickness increases; this indicates the enhancement in the device performance due to exciton confinement. If on the other hand, the emissive layer thickness is increased at fixed Ir-complex concentration, the probability of generating excitons increases too due to a higher probability of forming an exciton before carriers reach the opposite electrode, but the turn-on field looks the same at different EML thicknesses as shown in the Fig. 2(b) inset. These characteristics confirm the influence of the PVKH on the turn-on field and hence on the device efficiency.

As an initial device performance, an external quantum efficiency of 6.7%, current efficiencies of 23 cd/A, luminous efficacy of a source of 6.5 lm/W, and brightness of 7000 cd/m^2 were obtained at PVKH layer thickness of 20 nm and PVKL:PBD:Ir(ppy)$_3$ emissive layer thickness of 50 ± 3 nm (Fig. 3).

Further increase in device efficiencies was achieved by optimizing the EML thickness. Figure 4(a) shows the device EQE and brightness for devices with PVKH thickness fixed at 25 ± 3 nm and EML thickness varied from 35 to 105 nm. The EQE increases linearly with increasing the EML thickness up to ~80 ± 5 nm then drops sharply, while the brightness continues to increase. The drop in efficiency is mainly due to a cavity effect, but the rapid reduction also suggests a large shift in the balance of the charge carriers. However, the increase in the number of emitted photons indicates an increase in the exciton concentration but at lower efficiency. The corresponding EL profile for three selected EML thickness (37, 80, and 105 nm) is shown in Fig. 4(b). The normalized EL spectra emission was reconstructed using SETFOS 3.1 simulation software to extract information about the device efficiencies and the location of the emission zone. Figure 4(d) shows the simulation for the three thickness where the EL profile for a device with an EML thickness of 37 nm is not very sensitive to the dipole location, but it gives qualitatively a better match with the measured device efficiency when the emitting dipoles location are close to the PVKH/PVKL interface. The 80 ± 5 nm EML device required the emitting dipole location to be close to the PVKH/PVKL interface and show more sensitivity to the dipole location. Finally, the 105 nm device required dipole location to be very close to the PVKH/PVKL interface, and the EL profile is very sensitive to the dipole location. From the simulation of the EL profile, we concluded that the dipole location should be closer to the interface between the EML and PVKH to generate the observed EL profile. This is also shown in the simulation of the EML thickness swept from 20 to 150 nm for device with 25 nm PVKH [Fig. 4(c)], which confirms the dipole location and the observed optimum condition at device efficiency for EML thickness of 80 ± 5 nm. These results also confirmed that the PVKH layer is blocking the electrons and increasing the probability of forming excitons near the interface. However, a full comprehension of exciton distribution inside the EML layer requires a complete electronic-to-optical coupling simulation.

Figure 5 shows device efficiencies as a function of current density for EML thickness of 80 ± 5 nm and PVKH thickness of 25 nm. The maximum device EQE of 11%, device current efficiency DevE of 34 cd/A, luminous efficacy of a source LumE of 13 lm/W, and brightness of 11000 cd/m^2 has been obtained. Increasing device brightness depends

Downloaded 26 Sep 2012 to 129.234.252.67. Redistribution subject to AIP license or copyright; see http://jap.aip.org/about/rights_and_permissions

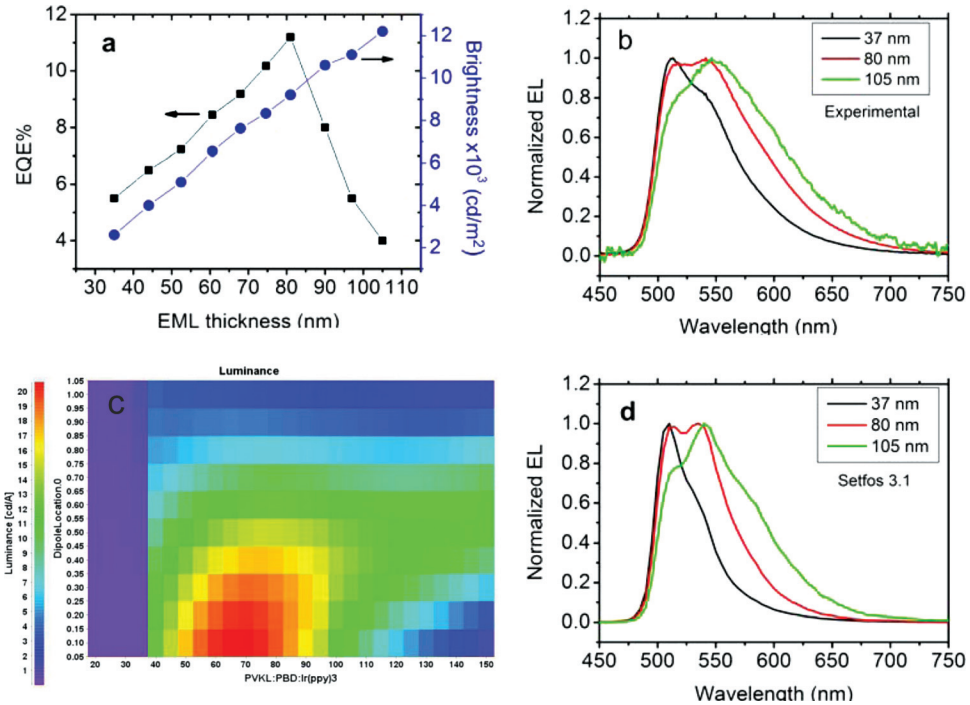

FIG. 4. (Color online) (a) Device EQE and brightness as functions of device EML thickness. (b) The corresponding EL profile for three selected thicknesses (37, 80, and 105 nm).

not only on the emissive exciton concentration but also on cavity optimization[19,20] and minimization of other quenching processes such as triplet-exciton quenching (triplet-triplet annihilation and triplet-polaron quenching)[28–30] and field induce quenching.[31] The EML layer thickness of 80 ± 5 nm gave the highest device efficiency, and is in agreement with the simulation results of Figs. 4(c) and 4(d). The dipole location of this EML is somehow shifted away from the interface.

D. Hole only device

It is important to know the effect of the HTL (PVKH) layer on the hole injection and transport and also on the energy level discontinuities that may occur between the two different molecular weight layers. Single carrier devices (hole only) are fabricated with a device structure: ITO/PEDOT:PSS/PVKH (0, 15, 32 nm)/PVKL:PBD:Ir(ppy)$_3$ (40 nm)/Au (100 nm). This structure ensures hole only injection because the potential barrier between the gold work function and EML is greater than 2.8 eV. Figure 6 shows the log–log plot of the voltage against current density where two distinct linear regions are indicated. At low voltage where the number of injected charge carriers is negligible compared to the number of thermally generated free carriers, n_o, the current density, J, is described by Ohm's law, $J = q\mu_e n_o V/d$, where q is the charge of the electron, μ is the electron mobility, n_0 is the thermally generated free carrier, and d is the active-layer thickness, and a slope of one has been obtained. At a voltage above 3 V, a second linear region appears with a slope of ~2, which indicates trap free space charge limited current (TF-SCLC)[32] $J = 9/8\mu\varepsilon V^2/d^3$, where ε is the permittivity of the polymer. The slopes look the same for all three devices; this indicates no energy level discontinuity induced by the PVKH layer and a smooth, "trap free" conduction occurs through the two PVK layers. Small current density enhancement occurs at the TF-SCLC region as the PVKH layer thickness increases up to 32 nm. These results also

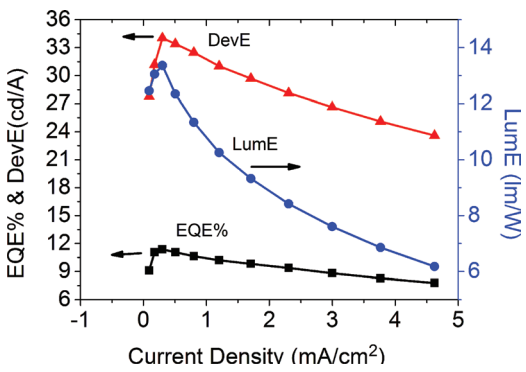

FIG. 5. (Color online) Optimized device efficiencies at HTL thickness of 25 nm and ELM layer thickness of 80 ± 5 nm.

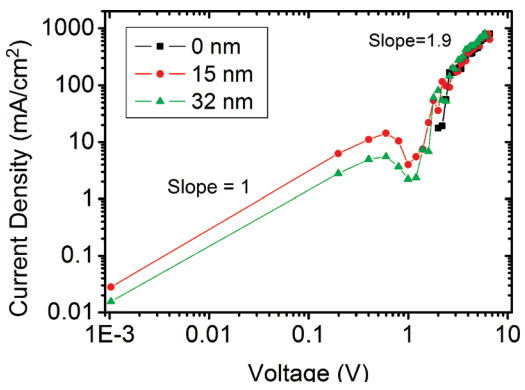

FIG. 6. (Color online) Log–Log plot for hole only devices at three different PVKH thicknesses.

Downloaded 26 Sep 2012 to 129.234.252.67. Redistribution subject to AIP license or copyright; see http://jap.aip.org/about/rights_and_permissions

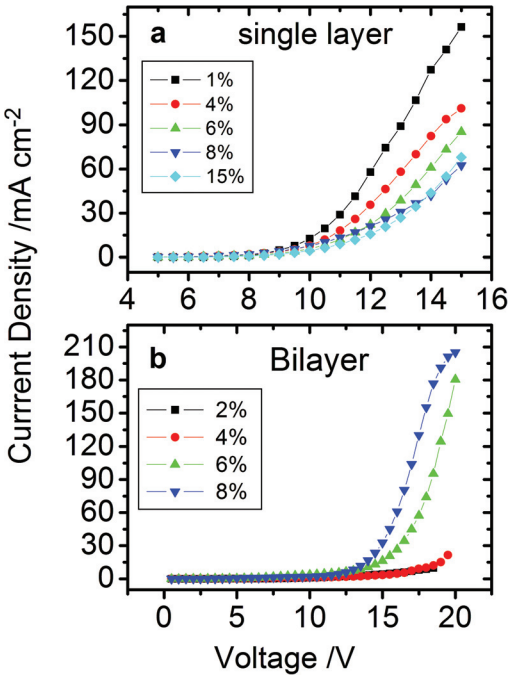

FIG. 7. (Color online) *J-V* characteristics for (a) single layer and (b) bilayer devices, PVKH(25 nm), PVKL(36mg/ml) at different dopant [$Ir(ppy)_3$] concentration.

indicate that the reduction in the current density as a function of PVKH thickness in the bipolar devices shown in Fig. 2 is due to the electron blocking by PVKH layer rather than by hole carrier reduction.

E. Dopant effect

Further investigation on the effect of the HT/EBL (PVKH) on device characteristics was conducted by studying the *J-V* characteristics for (a) single layer device (EML layer only) and (b) bilayer device PVKH/EML at various dopant (Ir $(ppy)_3$) concentrations. Figure 7 shows that the current density decreases with increasing dopant concentration in the single layer devices, whereas the bilayer devices show an increase in current density at higher dopant concentration. It is also shows that the rate of the current increase is higher in the bilayer device. To understand this behavior, the trap mechanism in the doped organic polymeric devices should be study. In the undoped organic layer, the charge carrier traps are states that energetically lie between the HOMO and the LUMO energy levels of the host. Trap states may have various origins such as material impurities or structural disorders.[33] The occupation of trap states depends on the free charge carrier densities and the trap depths, which are defined as the energetic distance of the trap state to the next transport site. In undoped organic materials, the trap depths are either shallow trap states originating from structural disorder in the organic layer or deeper trap states originating from impurities. If a highly purified (very low impurities) organic material is doped with a phosphorescent dye, such as heavy metal complex, the emissive energy state (the phosphorescent triplet exciton) forms a deep trap state for both electrons and holes, which dominate the organic layer trapping mechanism (here we assumed the organic host triplet is at higher energy than the phosphorescence triplet). Unlike the undoped organic light emitting devices where the recombination states are the organic singlet and the trap states are impurities or molecular disorders, in phosphorescence doped devices, the recombination states and the charge carrier's trap states now originate from the same energy states (the phosphorescent energy states). While the increase in the trap states in intrinsic organic devices reduces device efficiency, the increase in trap states in phosphorescent doped organic devices increases device efficiency (if no aggregation or excimer formation). In general, only Frenkel type excitons (spatially limited to one excited molecule) are efficient emissive exciton. Electrons and holes trapped individually at different complex molecules will not generate emissive excitons and therefore reduce device efficiency. The injected carriers are directly trapped[34] or indirectly trapped (by energy or charge transfer)[35] into the phosphorescence dopants. Therefore we may apply trap space charge limited current (TCLC)[36] to describe the bulk conductivity in the phosphorescent doped organic device. In general, the resulting trapped charge limited current (TCLC) model predicts a generally high exponent power law. In the presence of traps, as the forward bias is increased, the electron quasi-Fermi level rises toward the LUMO with increasing injected electron density. If traps are distributed in energy, they will be gradually filled with increasing field, and the current will increase faster than quadratic in SCLC until all traps are filled, yielding a high power law dependence of current on voltage as observed.

We will now explain the effect of the PVKH on the device electrical characteristics shown in Fig. 7. In the presence of the PVKH electron blocking layer, the confined free electrons in the EML layer increase and rapidly fill the trapping states, and the corresponding current increases much faster than for a single layer device as shown in Fig. 7. Figure 8 shows the *J–V* characteristics of Fig. 7 plotted on a log–log scale of a single layer and a bilayer device. Four different regions in each *J–V* curve can be identified. A full

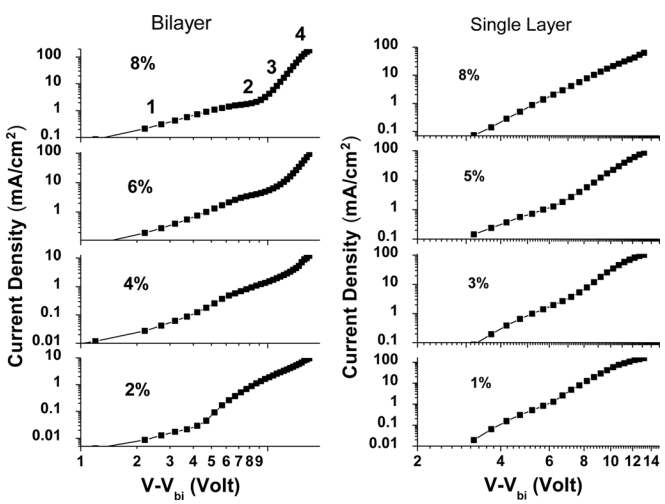

FIG. 8. Log–log plot of the applied voltage minus the build-up voltage V_{bi} against the device current density.

Downloaded 26 Sep 2012 to 129.234.252.67. Redistribution subject to AIP license or copyright; see http://jap.aip.org/about/rights_and_permissions

TABLE I. The slope of region 3 in the *J-V* characteristic of Fig. 8 for the single layer and bilayer devices.

	Bilayer				Single Layer			
Dopant concentration (%)	2	4	6	8	1	3	5	8
Slope of region 3	3.45	6.4	7.53	8.43	7.4	6.9	6.13	4.86

description of each region has been explained in our previous publication.[24] Here we are interested in region 3 where the TCLC model can be applied. Table I show the slope of region 3 obtained from Fig. 8, where the slope increases for bilayer devices and reduces for single layer devices. This result confirms the increase in the trapping efficiency in the bilayer devices and rapidly filling of the trapping states.

On the other hand, the increase or decrease in the current as a function of dopant concentration shown in Fig. 7 depends on two processes, (1) the trapping effect by the dopant that reduces current density and increases turn-on voltage at higher dopant concentration and (2) carrier transport enhancements, which increase as the dopant concentration increases due to the reduction in the hopping distance between the trapped carriers.[34] Carrier transport enhancement can also be thought of as a reduction in the trap energy state (deep to shallow trap energy level shift), which reduces the activation energy for the trapped carriers so enhances carrier mobility.[25] Thus the increase or the decrease in the overall device current density as a function of applied voltage depends on the competition between the two effects, and the *J-V* characteristic may turn from trapping dominant to transport regime as the dopant concentration change from low to high concentration.

F. Exciton quenching by the electrodes

Finally, the effect of the PVKH on the exciton quenching by the electrodes was also investigated using time resolved fluorescence photon counting. To estimate the quenching strength using time resolved photon counting, poly-spirobifluorene (PSBF) was selected as an emissive layer. We have selected this fluorescent material because a selective excitation wavelength can be provided by the second harmonic Ti-sapphire laser (372 nm) and also because its fluorescence lifetime is within the photon counting time resolved range (5 ps to 3 ns). The fluorescence decay lifetime of thin film of pristine PSBF without interfacing with electrodes or other polymer layers is 1 ns (Fig. 9). Interfacing PSBF with different device layers can offset the deleterious effects of various electrode structures on the quenching on

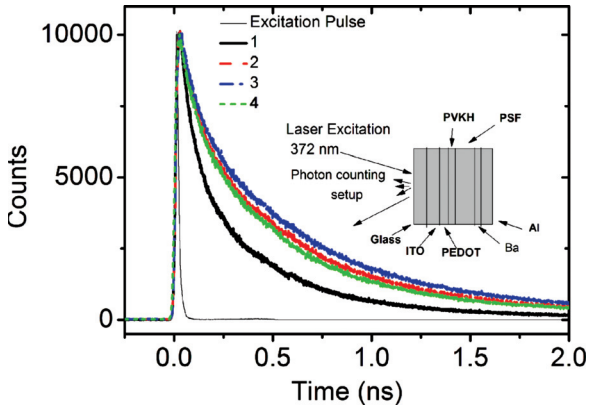

FIG. 9. (Color online) Decay time profile of PSBF layer at various multilayer configurations 1-4 (see Table I). The excitation wavelength was 372 nm; the emission wavelength was 420 nm. Inset: device structure and the photon counting set-up.

the emissive layer. Different sample configurations were prepared as shown in Table II. A device structure with the Ba/Al cathode was also tested without biasing to determine the quenching by the cathode (Ba/Al). The samples were illuminated by the laser beam from the glass side Fig. 9 inset. The excitation pulses wavelength was selected at 372 nm. PSBF has peak absorption at this wavelength while PVKH has no absorption at this wavelength; therefore, the laser pulse selectively excites the PSBF alone. Figure 9 shows the fluorescence intensity decay of the PSBF for various sample configurations. The decay profile was fitted using Globals analysis with three discrete exponential components,[37]

$$I(t) = \sum_{i=1}^{j} a_i \exp(-t/\tau_i)$$

where a_i represent the amplitudes of the components i at $t=0$, τ_i is the decay time of the component i. This analysis is necessary to isolate the fast decay components that reflect the quenching of the PSBF at the interface that is in contact with the other layers from the slow decay component that reflects the unquenched side of the PSBF located away from the contact zone. Table II shows the three decay components for the different sample configurations. The slowest decay component $\tau_1 = 1$ ns represents the unquenched PSBF, which is only slightly affected by the type of contact. The other two components, τ_2 andτ_3, are strongly influenced by the neighboring layers. The fastest component $\tau_2 < 60$ ps are the same for all different interfaces except for the device structure with the Ba cathode where very rapid quenching is

TABLE II. Emission decay components of PSBF for different multilayer configurations 1–4.

	Emission decay components									
Device configuration	a_1	τ_1	a_2	τ_2	a_3	τ_3	f_1	f_2	f_3	χ^2
1- G/ITO/PSBF	7.11	0.896	35.2	0.054	31.14	0.285	0.37	0.11	0.52	1.2
2- G/ITO/PEDOT/PSBF	10.33	1.126	18.17	0.059	27.59	0.384	0.499	0.046	0.45	1.1
3- G/ITO/PEDOT/PVKH/PSBF	11.37	1.187	15.41	0.06	26	0.408	0.54	0.037	0.42	1.04
4- G/ITO/PEDOT/PVKH/PSBF/Ba/Al	15.09	0.933	21.5	0.017	25.47	0.257	0.67	0.017	0.31	1.24

a_i, τ_i, and f_i, are the amplitude, decay time (ns), and fractional contribution to the steady state, respectively. χ^2 is the value of fit.

Downloaded 26 Sep 2012 to 129.234.252.67. Redistribution subject to AIP license or copyright; see http://jap.aip.org/about/rights_and_permissions

observed (17 ps). This implies that the cathode introduces a fast quenching channel; this is well known mirror quenching.[38] The intermediate component τ_3 around 250-400 ps clearly displays the effects of the ITO quenching. The actual quenching rate should be represented by the fractional contribution to the steady state parameter, f_i which is given by, $f_i = a_i\tau_i/\Sigma a_i\tau_i$.

Comparing the fractional contribution to the steady state parameters f_i for various sample configurations, we indicate that the major quenching source is the metallic electrodes (ITO and Ba). The parameters f_1 and f_3 indicate that the presence of the PVKH layer reduces only slightly the PSBF fluorescence emission quenching by the PEDOT:PSS. This implies that the enhancement in device efficiency in the present of the PVKH layer is mainly due to confining the exciton rather than prevent quenching by electrodes or the PEDOT:PSS.[23] The quenching by the Ba cathode in the device structure at zero voltage bias suggests that further introducing an electron transport layer (ETL) may enhance device performance by both preventing quenching by the cathode as well as facilitating electron injection. The electrodes' quenching strength depends on the emissive dipole location: better when the emissive dipole are away from both sides of interfaces. This can be achieved by better carrier balance. However, the PVKH layer in our system plays a major role in keeping the emissive dipole away from the PEDOT and the Ba/Al layers.

IV. CONCLUSIONS

In conclusion, a simple and generally applicable method of multilayer all solutions processable high efficiency polymer light-emitting devices based on different molecular weight polymer has been demonstrated. By using high molecular PVK as a hole transport electron blocking layer, effective electron blocking was achieved, which leads to an increase in exciton population in the phosphorescent zone. The use of low molecular PVK as a host material in the top layer prevents barrier formation for hole transport from the PEDOT to the EML and preserves hole continuity.

Furthermore, the HT/EBL (PVKH) layer prevents the EML from being in contact with the PEDOT. High molecular weight PVKH has a high resistivity to many solvents, so it is important to properly select the top layer solvent to reduce layer intermixing. Luminous efficacy of a source is poor (11 lm/W) due to poor hole and electron injection and can be increased by reducing the hole and electron injection barriers (higher PEDOT work function, replacing the Ba layer, introducing electron and hole injection layers, etc.). Increase in device efficiency with PVKH layer has also been tested using other emissive materials dissolved in toluene or xylene and shows a dramatic increase in device efficiency especially with materials posses high electron mobility. This may be considered as a universal method because the solubility of any polymer-solvent combination depends on the molecular weight of the polymer.[39] Devices with more than two layers are also possible and are under investigation given that different polymer molecular weights with different solvent strength or spinning methods are used.

ACKNOWLEDGMENTS

We would like to thank EPSRC for funding this work.

[1] D. J. Pinner, R. H. Friend, and N. Tessler, Appl. Phys. Lett., **76**, 1137 (2000).
[2] J. Kim, R. H. Friend, I. Grizzi, and J. H. Burroughes, Appl. Phys. Lett. **87**, 023506 (2005).
[3] X. Gong, S. Wang, D. Moses, G. C. Bazan, and A. J. Heeger, Adv. Mat. **17**, 2058 (2005).
[4] J. A. Hagen, W. Li, A. J. Stecki, and J. G. Grote, Appl. Phys. Lett. **88**, 171109 (2006).
[5] Q. Sun, D. W. Chang, L. Dai, J. Grote, and R. Naik. Appl. Phys. Lett. **92**, 251108 (2008).
[6] H. J. Bolink, E. Coronado, and M. Sessolo, Chem. Mater. **21**, 439 (2009).
[7] Y. Niu, M. S. Liu, J. Ka, and A. K. Jen, Appl. Phys. Lett. **88**, 093505 (2006).
[8] N. Rehmann, D. Hertel, K. Meerholz, H. Becker, and S. Heun, Appl. Phys. Lett. **91**, 103507 (2007).
[9] O. Solomeshch, Y. Yu, V. Medvedev, A. Razin, B. B. Ganon, Y. Eichen, J. Jin, and N. Tessler. Synth. Met. **157**, 841 (2007).
[10] B. Ma, F. Lauterwasser, L. Deng, C. S. Zonte, B. J. Kim, and J. M. J. Fréchet. Chem. Mater. **19**, 4827 (2007).
[11] S. Tseng, S. Lin, H. Meng, H. Liao, C. Yeh, H. Lai, S. Horng, and C. Hsu, Appl. Phys. Lett. **88**, 163501 (2006).
[12] K.-C. Tang, S.-R. Tseng, W.-S. Li, H.-F. Meng, S.-F. Horng, and C.-S. Hsu, Synth. Met. **158**, 287 (2008).
[13] R. Zhu, J.-M Lin, W.-Z. Wang, C. Zheng, W. Wei, W. Huang, Y.-H. Xu, J.-B. Peng, and Y. Cao, J. Phys. Chem. B **112**, 1611 (2008).
[14] J. Pina, J. S. de Melo, H. D. Burrows, A. P. Monkman, and S. Navaratnam, Chem. Phys. Lett. **400**, 441 (2004).
[15] C. Adachi, T. Tsutsui, and S. Saito, Appl. Phys. Lett. **57**, 531 (1990).
[16] See supplementary material at 126106 E-JAPIOU-109-126106 for Figs. S1–S3.
[17] G. E. Johnson, J. Chem. Phys. **62**, 4697 (1975).
[18] U. Giovanella, C. Bott, A. Papagni, R. Tubino, and L. Miozzo, Appl. Phys. Lett. **87**, 171910 (2005).
[19] E. Burrows, V. Khalfin, G. Gu, and R. Forrest, Appl. Phys. Lett. **73**, 435 (1998).
[20] Y. Fukuda, T. Watanabe, T. Wakimoto, S. Miyaguchi, and M. Tsuchida, Synth. Met. **111**, 155 (2000).
[21] SETFOS version 3.1, Fluxim, A. G. Dorfstrasse7, CH-8835 Feusisberg, Switzerland, 2010.
[22] H. A. Al-Attar, G. C. Griffiths, T. N. Moore, M. Tavasli, M. A. Fox, M. R. Bryce, and A. P. Monkman, Adv. Func. Mater. (to be published).
[23] H. Liu-Dong, L. Wei, D. Lian, and Q. Yong, Chin. Phys. Lett. **25**, 1457 (2008).
[24] R. W. T. Higgins, A. P. Monkman, H. G. Nothofer, and U. Scherf, J. Appl. Phys. **91**, 99 (2002).
[25] H. A. Al-Attar and A. P. Monkman, Adv. Funct. Mater. **16**, 2231 (2006).
[26] P. D'Angelo, M. Barra, A. Cassinese, M. G. Maglione, P. Vacca, C. Minarini, and A. Rubino, Solid-State Electron. **51**, 123 (2007).
[27] J. Kim, R. H. Friend, I. Grizzi, and J. H. Burroughes, Appl. Phys. Lett. **87**, 023506 (2005).
[28] C. Rothe H. A. Al Attar, and A. P. Monkman, Phys. Rev. B **72**(15), 9S (2005).
[29] K. Reineke, K. Walzer, and K. Leo, Phys. Rev. B, **75**, 125328 (2007).
[30] J. Kalinowski, W. Stamper, J. Mężyk, M. Cocchi, D. Virgili, V. Fattori, and P. D. Marco Phys. Rev. B **66**, 235321 (2002).
[31] J. Kalinowski, M. Cocchi, D. Marco, W. Stamper, G. Giro, and V. Fattori, J. Phys. D **33**, 2379 (2000).
[32] M. A. Lampert and P. Mark, *Current Injection in Solids* (Academic, New York, 1970), Chap. 3.
[33] A. J. Campbell, D. D. Bradley, and D. G. Lidzey. J. Appl. Phys. **82**, 6326 (1997).
[34] Y. Y. Noh, C. L. Lee, J. J. Kim, and K. Yase, J Chem. Phys. **118**, 2853 (2003).
[35] C. G. Yahioglu, P. Le Barny, R. H. Friend, and N. Tessler, Adv. Mater. **11**, 285 (1999).
[36] A. J. Campbell, D. C. Bradley, and D. G. Lidzey, J. Appl. Phys. **82**, 6328 (1997).
[37] E. Gratton and J. Beechem, *Globals WE, Globals for Spectroscopy* (The Laboratory for Fluorescence Dynamics, Irvine, CA, 2004).
[38] P. T. Worthing, R. M. Amos, and W. L. Barnes, Phy. Rev. A **59**, 865 (1999).
[39] K. Adamska and A. Voelkel, J. Chromatogr. A **1132**, 260 (2006).

Downloaded 26 Sep 2012 to 129.234.252.67. Redistribution subject to AIP license or copyright; see http://jap.aip.org/about/rights_and_permissions